Hadronic interactions and primary-cosmic-ray composition at energies around $10^{15}-10^{16}$ eV derived from the analysis of high-energy gamma families

J. R. Ren, A. X. Huo, S. L. Lu, and S. Su
Institute of High Energy Physics, Academia Sinica, China

C. R. Wang, N. J. Chang, P. Y. Cao, J. Y. Li, and B. T. Zou
Department of Physics, Shangdong University, China

S. Z. Wang
Department of Physics, Zhengzhou University, China

G. Z. Bai, Z. H. Liu, G. J. Li, and Q. X. Geng
Chongqing Architecture College, China

R. D. He and W. D. Zhou
Department of Physics, Yunnan University, China

M. Amenomori and H. Nanjo
Department of Physics, Hirosaki University, Japan

N. Hotta and I. Ohta
Faculty of Education, Utsunomiya University, Japan

K. Mizutani
Department of Physics, Saitama University, Japan

K. Kasahara and T. Yuda
Institute for Cosmic Ray Research, University of Tokyo, Japan

T. Shirai, N. Tateyama, and S. Torii
Faculty of Technology, Kanagawa University, Japan

M. Shibata
Faculty of Education, Yokohama National University, Japan

H. Sugimoto and K. Taira
Sagami Institute of Technology, Japan
(Received 18 November 1987)

Gross features of gamma families observed at Mt. Kanbala (5500 m above sea level) and Mt. Fuji (3750 m) are summarized in comparison with a Monte Carlo simulation based on a plausible assumption about hadronic interactions and primary composition. Our analysis shows that the assumption of approximate Feynman scaling in the fragmentation region and a heavy-enriched primary composition in the energy range over 10^{15} eV is wholly compatible with the experimental data. That is, there is no evidence of strong violation of Feynman scaling in the fragmentation region at least up to 10^{16} eV. As to the primary cosmic rays, our data infer a steepening of proton spectrum at energies around 10^{14} eV. The proton component in the primary cosmic rays is estimated to occupy 15–20% of the total flux at 10^{15} eV. Some other interesting implications on hadronic interactions are discussed with reference to the structures of gamma families.

I. INTRODUCTION

High-energy hadronic interactions have been studied in the energy region over several thousand TeV at Mt. Kanbala (5500 m, China-Japan Collaboration[1]) and Mt. Fuji (3750 m, Mt. Fuji Collaboration[2]) with large-scale emulsion chambers. These experiments enable us to observe many instances of events called a "family," which is a bundle of high-energy particles originated by a high-energy cosmic ray in the atmosphere. The study of these family phenomena is the key subject of emulsion-chamber experiments at mountain altitudes. In previous papers,[1,2] we have suggested the following about hadronic interactions in the energy region around 10^{15} eV based on the re-

sults from our emulsion-chamber experiments: no strong violation of Feynman scaling in the fragmentation region, increasing inelastic cross sections with energy as $\sigma_{in}(p\text{-air}) = 290(E_0/1\ \text{TeV})^{0.06}$ mb (E_0 stands for the primary energy in units of TeV), and implication of drastic increase of high-P_t jet production. On the composition of primary cosmic rays we have shown evidence supporting a steepening of proton flux at energies around 10^{14} eV, especially with the result of increasing fraction of heavy nuclei in the energy region of $10^{15}-10^{16}$ eV.

Since 1982 extensive data have been accumulated about hadronic interactions from CERN SPS collider experiments[3] in the energy region from $\sqrt{s} = 200-900$ GeV, corresponding to the energy range from $E_0 = 2\times10^{13}$ to 4×10^{14} eV in the laboratory system. Then, the modeling of hadronic interactions at ultrahigh energies becomes easier as compared with that at several years ago. There is, however, still controversy on the validity of Feynman scaling in the fragmentation region because of a lack of information about high-energy particles which are most likely emitted in very narrow angles contained in the beam pipes. This problem might be irrevocably settled only by cosmic-ray experiments since the difficulty of measuring those particles becomes more and more keen with increasing accelerator energies. However, it is estimated that the violation is in the level of 10–15 % at energies around 10^{14} eV, if any. Also, the dramatic increase of high-P_t jets seems to be well described by QCD predictions.[3]

With rapid rising of current accelerator energies, our interest is now starting for investigating the cosmic-ray phenomena observed in the energy region of $10^{16}-10^{17}$ eV (Ref. 4). In such an ultrahigh-energy region, emulsion-chamber experiments at high mountain altitudes are still expected to provide reliable information about hadronic interactions. Novel analysis of superfamilies with energy higher than 1000 TeV may be able to catch signs of new phenomena beyond expectation in very near future.

On the other hand, the advent from the $\bar{p}p$ collider results has also increased the potential for understanding the mass composition of primary cosmic rays in $10^{15}-10^{17}$ eV (Ref. 5), an almost inaccessible energy region with any kind of direct measurements for the time being.

For the past several years, new data have been obtained from the Mt. Kanbala experiment and also statistics of the Mt. Fuji data have been increased significantly by the increased exposure time. In this paper we examine the gross features of family events observed by both experiments, and clarify how these are entangled with hadronic interactions and primary composition. In Sec. II the experimental procedure is briefly reviewed. Section III is used for introducing the assumption of our Monte Carlo simulations. Some of the predictions are summarized from the Monte Carlo simulations in Sec. IV. The experimental results are presented in Sec. V in comparison with the Monte Carlo simulations. Finally Sec. VI is devoted to summarizing what can be asserted about hadronic interactions and composition of primary cosmic rays at energies around $10^{15}-10^{16}$ eV.

II. EXPERIMENT

The emulsion chambers used in both experiments at Mt. Kanbala and Mt. Fuji have a multilayered structure of metal plates (absorber material) and photosensitive layers, as schematically shown in Fig. 1. Photosensitive layers, each of which generally contains two sorts of x-ray film with a different sensitivity, are put every 2 cascade units (cu) of metal plates in the chamber.[5,6] Two types of emulsion chamber have been exposed in both experiments. One is thin and of large area for observing family events with energy as high as possible (total thickness of absorber is less than 14 cu). The other type is thick for observing family events containing hadrons among their members (in the Mt. Kanbala experiment both lead and iron plates are used as absorber material).

A high-energy shower is recorded as a series of black spots on the x-ray films ranging over several layers in an emulsion chamber. The energy of each shower found in the chamber is estimated by measuring the change of optical density of shower spots registered in the x-ray films extending over several layers on every shower, and comparing it with a calculation based on the cascade theory and the sensitivity of x-ray films. The overall accuracy of energy determination is estimated to be about 20% around several TeV of shower energy.[5,6]

A family event is easily identified by confirming that the showers of family members are parallel to each other. Cascade showers in each family are statistically classified into two groups: gamma rays (abbreviation of electromagnetic components) and hadrons. In both experiments gamma rays are defined as showers with starting depth less than 6 cu, but with no accompanying successive interactions in the chamber, and others are treated as hadrons. The minimum energy of showers assigned to be family member is set to 4 TeV in this paper. Then, family events are divided into two classes, i.e., "gamma families" and "hadron families." The former is composed of only gamma rays and the latter of both gamma rays and hadrons, which are essentially observed in the thick-type chambers.

To date, we have finished the exposure of 420 m^2yr at Mt. Kanbala and 1000 m^2yr at Mt. Fuji, respectively.

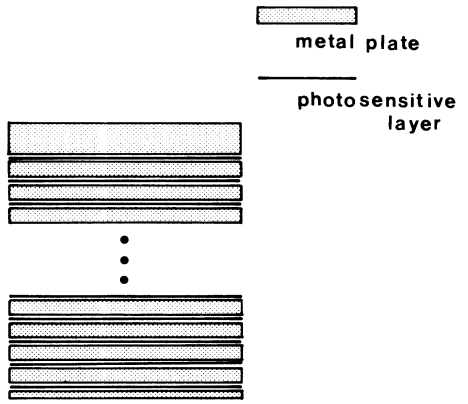

FIG. 1. The typical structure of an emulsion chamber.

Then the number of family events observed amounts to 80 events ($\sum E_\gamma \geq 200$ TeV) at Mt. Kanbala and to 220 events ($\sum E_\gamma \geq 100$ TeV) at Mt. Fuji, respectively. In this paper, we discuss the properties of gamma families on the bases of these data sets. Gross features of hadron families will be presented elsewhere.[7]

III. MONTE CARLO SIMULATION

Since statistical fluctuations in the interaction processes, together with experimental bias, deform the family phenomena observed with mountain emulsion chambers considerably, a Monte Carlo simulation is indispensable to derive reliable conclusions from experimental data.

The energy of primary particles we are now concerned with almost falls into the range between 10^{15} and 10^{17} eV. Therefore, the speculation is inevitably attended with some ambiguities about hadronic interactions. Furthermore, the problem becomes manifold by the fact that no direct measurements of the nuclear composition of primary-cosmic-ray components are available above 10^{14} eV. The only way for overcoming all these difficulties is to examine whether or not the reasonable extrapolation of particle interaction properties beyond accelerator energies is totally compatible with experiments. The model used must be always brushed up through a feedback process in comparison with available experimental results.

The models examined in our simulation calculation are almost the same as those in our previous papers,[2,8] but some parts are refined to the latest ones as follows.

A. Hadronic interactions

We adopted mainly the scaling interaction model which is made so as to fit to the accelerator data from 100 GeV to 400 TeV (CERN SPS Collider).[3] That is, our assumption is essentially based on that high-energy hadronic interactions consist of low-P_t soft processes and high-P_t hard scattering which are described by Feynman scaling and perturbative QCD, respectively. This model predicts that Feynman scaling violates rather strongly in the central region, but mildly in the fragmentation region ($x \gtrsim 0.05$) as learned from Fig. 2, where $x = E/E_0$, and E and E_0 are the energies of secondary and primary particles, respectively. The degree of shrinkage of x distribution is observed to be at most a factor of 1.7, defined by the ratio

$$R_s = \frac{[x\, dn(E_0 = 10^{12}\ \text{eV})/dx]_{x=0.3}}{[x\, dn(E_0 = 10^{16}\ \text{eV})/dx]_{x=0.3}} ,$$

when the energy goes up from 10^{12} to 10^{16} eV.

The multiplicity from the soft process obeys Koba-Nielsen-Olesen (KNO) scaling with the average multiplicity depending on the energy as $a + b \ln E_0 + c \ln^2 E_0$ while the total multiplicity including hard scattering shows a strong energy dependence like $\langle n \rangle = 18 \times E_0^{0.17}$, where E_0 stands for the primary energy in unit of TeV.

The inelastic cross sections are assumed to increase with energy as $\sigma_{\text{in}}(p\text{-air}) = 290(E_0/1\ \text{TeV})^{\delta}$ mb and $\delta = 0.06$. We denote this model as SQI (scaling, QCD, and increasing cross section).

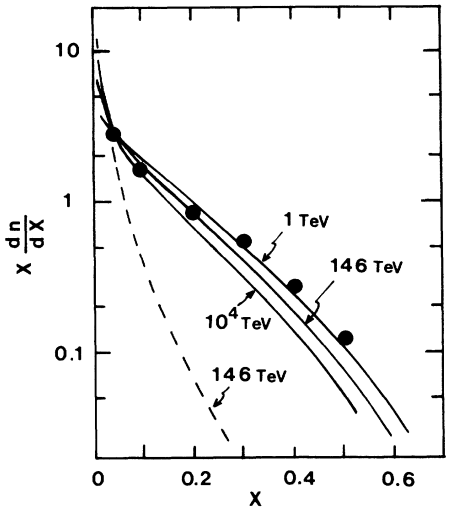

FIG. 2. x distribution of secondary pions produced by proton-proton interaction at various energies used in the scaling model. In actual cases the target effects are adequately taken into account. The case of the fireball model is also shown by the dotted line. Closed circles are the accelerator data at 250 GeV (Ref. 9).

We also examined the fireball model (referred to as F) to appraise the effects of strong violation of Feynman scaling in the fragmentation region though this model is already denied because of incompatibility with accelerator data.[3] The total multiplicity is normalized to the accelerator data at 10^{14} eV, and below this energy the fireball model is smoothly connected to the scaling one mentioned above.

The P_t distribution in the soft processes is assumed to obey a function of linear exponential form with $\langle P_t(x=0) \rangle = 330$ MeV/c at 10^{12} eV. High-P_t jets are adequately incorporated by perturbative QCD. We can also show that the two processes well reproduce the CERN SPS collider data.[8]

B. Primary spectra and composition

As shown in the Monte Carlo simulation,[2] the mean primary energy responsible for making gamma families with $\sum E_\gamma = 100$ TeV at high mountain altitude is estimated to be $(3-5) \times 10^{15}$ eV for protons. Also it should be noted that the fraction of protons in the primary plays an important role in investigating the gross features of family phenomena since its production efficiency strongly depends on the primary energy per nucleon for nuclei. Unfortunately, however, at present we have only deficient information about primary cosmic rays, especially primary mass composition in the energy region from 10^{14} to 10^{17} eV. A smooth connection of total primary spectra between direct observations[10] at lower energies and air-shower observations[11] at higher energies seems to imply a change of slope between 10^{15} and 10^{16} eV, the differential exponent increasing from about 2.6 to 3.0–3.2 which is sometimes called the "knee."[12] The origin of the "knee" is still under debate. On this account, this energy region

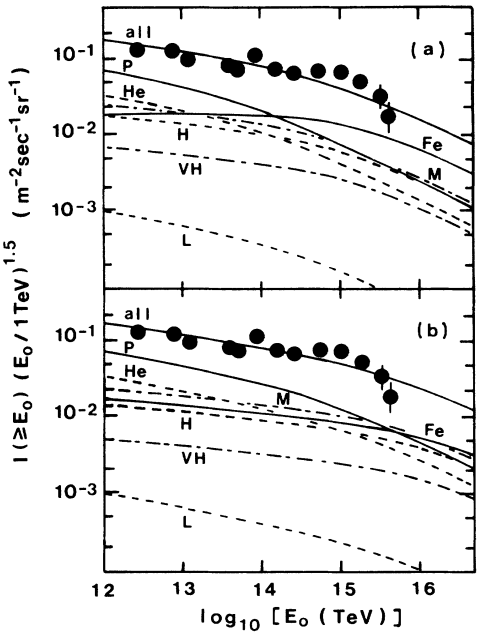

FIG. 3. (a) Primary-cosmic-ray composition assumed in the simulation for the model HDSQI (MSQI). Solid circles are the data by Grigorov *et al.* (b) Same as (a), but for the model PDSQI.

is of considerable importance for discriminating different models of origin, propagation, and acceleration mechanisms of cosmic rays in the Galaxy. Plausible models[13] involving shock acceleration mechanism, for example, predict a universal spectral slope and a rigidity-dependent steepening above 10^{14} eV. Then a change is naturally expected in the mix of primary elemental species over this energy region. In the modeling of the primary cosmic rays we use the p, He, CNO, light-heavy (LH), and Fe spectra directly measured in the low-energy region,[10] say $\lesssim 10^{12}$ eV/nucleon, and a rigidity-dependent steepening is assumed for the energy spectrum for various nuclei at higher energies. The absolute intensity of all particle spectrum is normalized to Grigorov's satellite data[14] at energies around 10^{14} eV.

Two different models for the primary cosmic rays are examined critically in the Monte Carlo simulation, as shown in Figs. 3(a) and 3(b). Here, Fig. 3(a) is the case in which a bending energy of protons (E_b) is taken to be

TABLE I. Fraction of each component in the assumed primary-cosmic-ray spectrum in Figs. 2(a) and 2(b). LH, MH, H, and VH mean light-heavy, medium-heavy, heavy, and very heavy nuclei, respectively.

Primary	E_0 (eV)	10^{14} (%)	10^{15} (%)	10^{16} (%)
HDSQI	P	26	18	14
(MSQI)	He	14	10	8
	L-MH	19	18	17
	H	13	15	14
	VH	5	6	7
	Fe	23	33	40
PDSQI	P	34	27	20
	He	17	14	12
	L-MH	19	22	23
	H	12	14	16
	VH	4	5	6
	Fe	14	18	23

10^{14} eV and an iron component has a spectrum flatter than the others [referred to as heavy-dominant (HD) or M]. On the other hand, in Fig. 3(b) the proton spectrum is assumed to become steeper at $E_b = 10^{15}$ eV [proton-dominant (PD)]. In both cases, the spectral index for every nucleus becomes -3.0 in a differential form over the bending point in order to meet with air-shower data. The fraction of each component at energies 10^{14}, 10^{15}, and 10^{16} eV is summarized in Table I.

In addition to the above cases, we also examined the primary cosmic rays composed of proton only in all energy regions (p). Its absolute intensity, however, is adjusted so as to take a half value of the Grigorov all-particle data at 10^{14} eV, with a bending point at $E_b = 10^{15}$ eV. Of course the most efficient yield of families is expected in this case.

In Table II all the models examined in this paper are briefly described. In the following a symbol listed in this table is used to stand for a model, such as HDSQI.

IV. METHOD OF ANALYSIS AND CONJECTURE FROM THE MONTE CARLO SIMULATION

In the target diagram of a family are usually observed substructures which may be called clusters. Mathematically such a cluster is defined to be a group of particles

TABLE II. Summary of the models examined by Monte Carlo simulation. Details are described in the text.

Interaction	Cross section	Primary	Symbol
Scaling (S)	increasing (I)	p	PSQI
+		PD	PDSQI
QCD jets (Q)		HD	HDSQI
Fireball (F)[a]	increasing (I)	p	PFQI
+		PD	PDFQI
QCD jets (Q)		HD	HDFQI

[a]For $E_0 < 10^{14}$ eV, fireball (F)→scaling (S).

having similarity which is expressed by how short the distance between them is, and its technique was developed in the previous paper.[2] Here we again apply this clustering method to every gamma family in order to coalesce high-energy showers into clusters, each of which hopefully will recover information degraded by electromagnetic cascading in the atmosphere. For this, one calculates $\chi_{ij}=(E_iE_j)^{1/2}R_{ij}$ between observed showers for all pairs of showers in a family. If χ_{ij} is less than a given cutoff value χ_c then the ith and the jth shower are combined into a "cluster" with an energy E_i+E_j and a new vector position for their energy weighted centroid, where $E_{i(j)}$ stands for the energy of the ith (jth) shower and R_{ij} the geometrical distance of the ith and the jth clusters. The process is terminated when $\chi_{\min}\geq\chi_c$ or $N_c=1$. The value of the cutoff parameter χ_c can be reasonably chosen to be 40 TeV cm at Mt. Fuji and 45 TeV cm at Mt. Kanbala, respectively. The gamma families obtained from the experiments and the simulation calculations were rejuvenated under the same clustering conditions.

In Fig. 4 is shown the cluster number distribution of gamma families with energies $\sum E_\gamma\geq 100$ TeV. The Monte Carlo data are from the model HDSQI and the experimental data are taken from the Mt. Fuji experiment. A good agreement is noticed between the experiment and the simulation in this figure. The simulation result also teaches us that gamma families originated from heavier primaries tend to exhibit large cluster number N_c as compared to those from proton-initiated families. Then, a set of gamma families is divided into two classes according to their cluster number N_c, i.e., class 1 is a group composed only of gamma families with $N_c\leq 5$, but class 2 is that with $N_c\geq 8$. The dissection of Monte Carlo results reveals that almost all the families ($>80\%$) in class 1 are surely generated by protons. The characteristic features of gamma families in each class are summarized in Table III. The effects of heavier nuclei would be examined through the analysis of the families in class 2.

In the following section the experimental results about gamma families observed at Mt. Kanbala and Mt. Fuji are discussed for clarifying the gross features of hadronic interactions at energies around several thousand TeV as well as the composition of primary cosmic rays around the "knee."

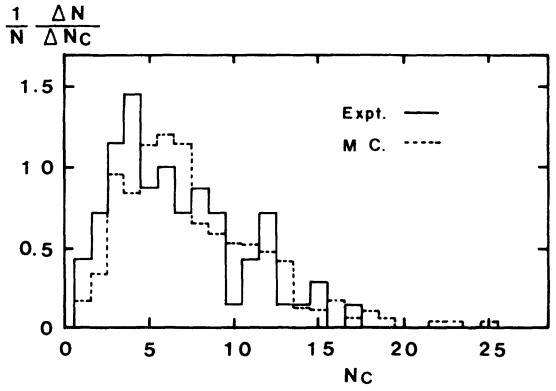

FIG. 4. Cluster number distribution in the gamma families with $\sum E_\gamma\geq 100$ TeV, observed at Mt. Fuji. The Monte Carlo result by the model HDSQI is compared with the experimental data.

V. RESULTS AND DISCUSSIONS

A. Energy-flow spectra of gamma families

The intensity of gamma families is known to depend sensitively on the increase of cross sections, inelasticity, and also on the composition of primary cosmic rays. In Figs. 5(a) and 5(b) are presented the energy-flow spectra of gamma families observed at Mt. Kanbala and Mt. Fuji, respectively.

The intensity difference of gamma families observed at Mts. Fuji and Kanbala gives a value of 110 ± 10 g/cm^2 for the attenuation length of gamma families in the atmosphere, which is consistent with the value obtained from the zenith angle distribution of gamma families at Mt. Fuji.[2] This value is sensitive to the increasing rate of cross sections of primary protons in the atmosphere, but is almost free from the absolute intensity and the mass composition of primary cosmic rays, as discussed in Refs. 2 and 15. The experimental result obtained is proved to be consistent with the increasing rate of $\delta=0.06$ assumed in the simulation.

The experimental data on the absolute intensity of gamma families are compared with the simulation results of different models. One sees that the model HDSQI nicely fits to experimental data at both Mt. Fuji and Mt.

TABLE III. Some characteristic features of gamma families consisting of $N_c\leq 5$ and $N_c\geq 8$. In this table, E_0 stands for the energy of primary cosmic rays.

$\sum E_\gamma$ (TeV)	$\left\langle\sum E_\gamma\right\rangle$ (TeV)	Fraction (%) [$\langle E_0$/nucleon$\rangle$ (TeV)] p	He	$>$CNO
		Class 1 ($N_c\leq 5$)		
100–200	150	82 [3500]	9	9
200–1000	300	93 [6200]	7	
		Class 2 ($N_c\geq 8$)		
100–200	180		17 [2100]	83 [1000]
200–1000	450	50 [18000]	23 [4000]	27 [2500]

Kanbala. Under the assumption of a slowly increasing cross section, $\delta=0.04$, the calculated fluxes increase by a factor of 1.5–1.7. On the other hand, the model PSQI is completely ruled out by a similar comparison, giving higher intensities by a factor of 5. The model PDSQI still gives a higher intensity by a factor 2–2.5 than the experiments as shown in Fig. 5. To put it in other words, emulsion-chamber data are incompatible with the primary composition of proton dominant around and over

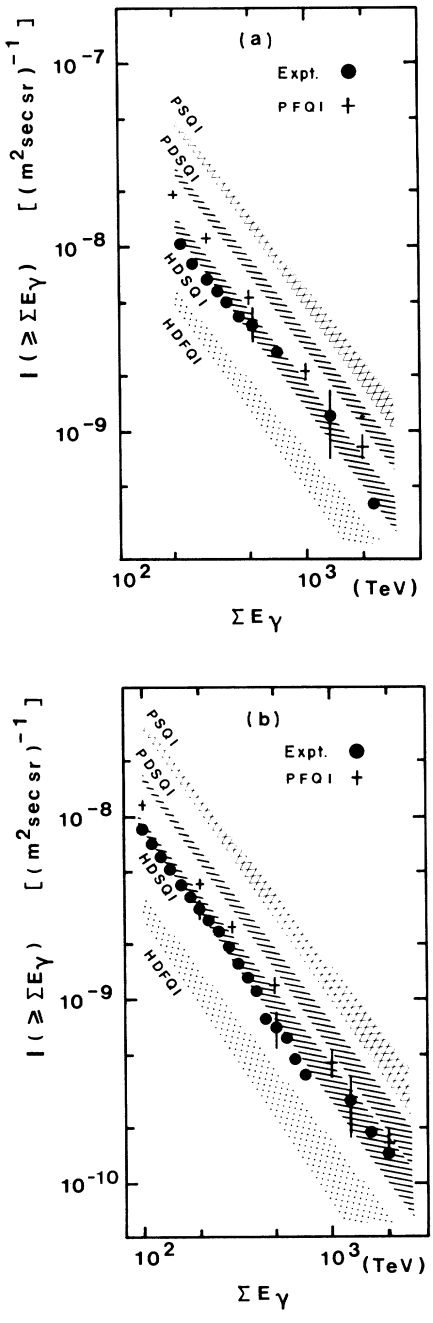

FIG. 5. (a) Integral energy-flow spectrum of gamma families at Mt. Kanbala. Simulation results of the PSQI, PDSQI, HDSQI, PFQI, and HDFQI models are presented to be compared with the experimental data. (b) Same as in (a), but for the experimental data of Mt. Fuji.

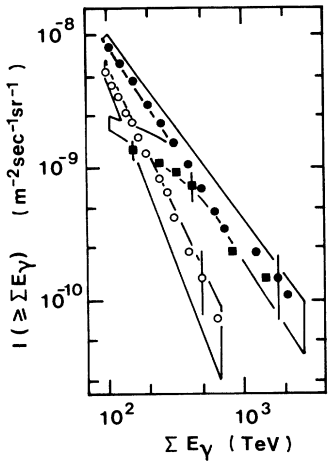

FIG. 6. Integral energy-flow spectra of gamma families composed of $N_c \geq 1$ (solid circles), $N_c \leq 5$ (open circles), and $N_c \geq 8$ (solid squares), respectively, observed at Mt. Fuji. Simulation result is from the model HDSQI (areas bounded by solid lines).

the "knee," proposed especially by some authors.[16,17]

Of course, a strong scaling breakdown can be forcibly met with the experiments by assuming the primary cosmic rays of proton dominance shown in Fig. 3(b) or more. This situation may be easily understood from Fig. 4 where the energy-flow spectrum expected from the model PFQI is presented as an example. However, such a high-multiplicity model has difficulty in interpreting the data on multicore events as will be discussed in Sec. IV E.

The sensitivity to the average atomic mass of the primary cosmic rays would also be perceived more directly by the data shown in Fig. 6, where the intensities of gamma families composed of given numbers of cluster are compared with the simulation results from the model HDSQI. A noteworthy fact is that the intensity of gamma families with $N_c \leq 5$ is very sensitive to the proton content in the primary cosmic rays. A good agreement seen in Fig. 6 evidently supports that a dominance of proton components is unacceptable in the primary cosmic rays at energies around the knee.

As a whole, it is concluded that approximate Feynman scaling in the fragmentation region incorporated with the heavy enriched primary around the knee well explains the intensities of gamma families observed both at Mt. Kanbala and Mt. Fuji.

B. f' and n' spectra of "proton"-induced gamma families

A previous paper[2] presented the f' and n' spectrum of gamma families in the energy region over $\sum E_\gamma \geq 100$ TeV, which are observed by the Mt. Fuji experiment. Here, $f'=E_\gamma / \sum' E_\gamma$, where $\sum' E_\gamma$ stands for the energy sum of gamma rays in order of energy satisfying the condition $f' \geq f'_m$ and f'_m is fixed to be 0.04 in the present analysis. Then, n' means the number of constituent gamma rays with $f' \geq f'_m$ in a family. From this procedure it is easily understood that these spectra well reflect the behavior of the high-energy part of the gamma rays in the families. However, as discussed already, the sensitivity to

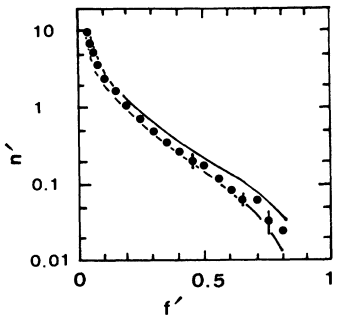

FIG. 7. f' spectrum of gamma families with $\sum E_\gamma \geq 100$ TeV and $N_c \leq 5$. Simulation result of the model HDSQI (area bounded by solid lines) is compared with the experimental data (solid circles) obtained at Mt. Fuji.

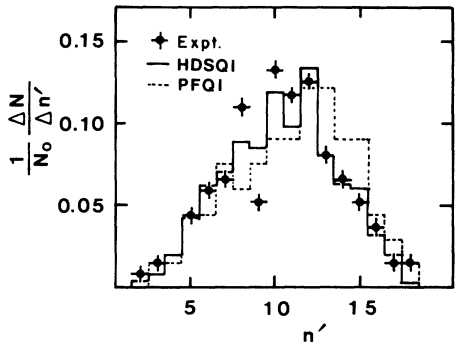

FIG. 9. n' distribution of gamma families with $\sum E_\gamma \geq 100$ TeV and $N_c \leq 5$ at Mt. Fuji is compared with the simulation results of the HDSQI and PFQI models.

the change of hadronic interactions and primary composition is strongly masked by successive cascade processes of gamma rays in the atmosphere.

In spite of this it is still interesting to examine the f' and n' spectrum, especially for gamma families which are expected to be originated by protons. In Fig. 7 is shown the f' spectrum of those gamma families with $N_c \leq 5$ in the energy region of $\sum E_\gamma > 100$ TeV observed at Mt. Fuji. The f' spectrum for all gamma families in the same energy region is also presented in Fig. 8 for both experiments at Mt. Kanbala and Mt. Fuji. It is well confirmed that there exists no difference on the f' spectra between the models HDSQI and PFQI. In both figures, therefore, a comparison is made with the Monte Carlo result from the model HDSQI being compatible with the experimental data.

The n' spectrum at Mt. Fuji is displayed in Fig. 9 to be compared with the model HDSQI and PFQI. Much difference is seemingly hard to find between two models. The mean multiplicity $\langle n' \rangle$ is, however, obtained as 9.5 ± 0.4, 9.2 ± 0.3, and 10.3 ± 0.4 for the experiment, the model HDSQI, and the model PFQI, respectively, so that a better agreement may be met with the model HDSQI.

These facts discussed above may be additional evidence that the experimental data are compatible with the scaling model. This problem is again examined in connection with the lateral spreads of gamma rays.

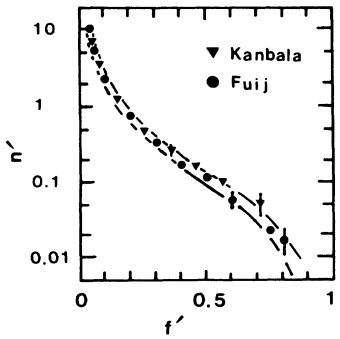

FIG. 8. f' spectra of gamma families with $\sum E_\gamma \geq 100$ TeV observed at Mt. Kanbala and Mt. Fuji. Simulation result is from the HDSQI model (area bounded by solid lines).

C. Lateral spreads of gamma families

Lateral spreads of gamma families are sensitive to the transverse momentum of secondary particles produced by hadronic interactions. In Figs. 10(a) and 10(b) are shown the scatter plots of the spread of gamma rays, $\langle R \rangle$ and $\langle ER \rangle$, and the sum energy $\sum E_\gamma$ for gamma families observed at Mt. Fuji and Mt. Kanbala, respectively. The mean lateral spreads of gamma families in the respective energy interval of $\sum E_\gamma$ are compared with the simulation results from the HDSQI and PFQI models. In this comparison we should call attention that the observed lateral spreads $\langle R \rangle$ inevitably have a tendency to become smaller as compared with the real ones because some isolated showers far from the family center are sometimes failed to be identified as family members, while the $\langle ER \rangle$ values are rather free from this experimental bias. Taking this into account, comparisons made in Fig. 10 show substantially in favor of the model HDSQI.

The distribution of the mean lateral spread $\langle R \rangle$ of each family in the energy interval of $\sum E_\gamma = 200-400$ TeV is compared with the HDSQI model in Fig. 11. Wide-ranging scattering of the lateral spreads seen in Fig. 10 is also confirmed to be within the scope of expectation of this model.

The lateral spreads of gamma families with $N_c \leq 5$ and $N_c \geq 8$ are displayed in Figs. 12(a) and 12(b), respectively. The distribution of the mean lateral spread $\langle R \rangle$ of each "proton"-induced gamma family with $N_c \leq 5$ is also compared with the model HDSQI in the energy interval of $\sum E_\gamma = 100-1000$ TeV in Fig. 13. The lateral spreads of gamma families $\langle R \rangle$ and $\langle ER \rangle$ and their dispersions are shown to be wholly compatible with the scaling model. In particular it is well recognized that apparent disagreement on the lateral spreads $\langle R \rangle$ seen in Fig. 10 is fairly diminished in Fig. 12(a) since the gamma families with smaller lateral spreads are preferentially selected by imposing the condition $N_c \leq 5$. In particular substantial agreement between the experiment and the Monte Carlo simulation seen in Fig. 12(a) would strongly support that the increasing rate of $\langle P_t \rangle$ with energy is rather mild. The simulation can predict that the mean $\langle P_t \rangle$ of secondaries takes a value of 500–550 MeV/c at energies

around 10^{16} eV, but a smaller value in the fragmentation region. As a matter of fact, a dramatic increase of QCD jet production is expected at such a high-energy region. But, the propagations of cosmic rays in the atmosphere are mainly controlled by secondary particles produced in the fragmentation region, with the result that the effect of QCD jets to the lateral spreads is 10% at most in our concerned energy regions. That is, most QCD jets are attributed to gluon-gluon collisions generating a great number of soft pions whose energies are rapidly dissipated before reaching detectors. Consequently, QCD jets only give a minor contribution to the cosmic-ray propagations in the atmosphere.

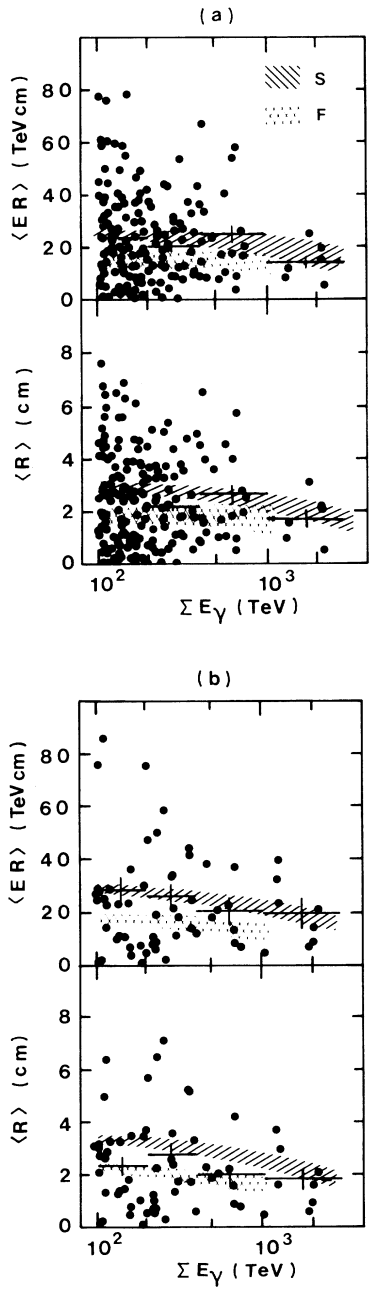

FIG. 10. (a) Scatter plots of lateral spread of gamma rays, $\langle R \rangle$ and $\langle ER \rangle$, in each gamma family and sum energy $\sum E_\gamma$, observed at Mt. Fuji. Mean lateral spreads averaged in respective energy region of $\sum E_\gamma$ are compared with the simulation results of the model HDSQI (S, shadow area by oblique lines) and PFQI (F, cross lines). (b) Same as in (a), but experimental data are from the Mt. Kanbala experiment.

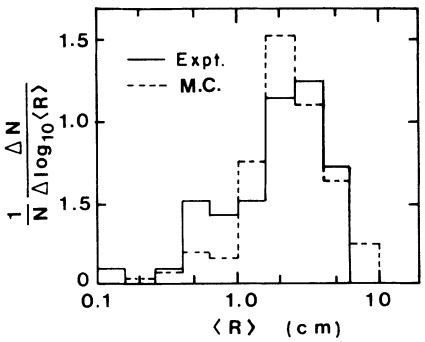

FIG. 11. Distribution of mean lateral spread $\langle R \rangle$ of each gamma family in the energy region of $\sum E_\gamma = 200$–400 TeV, observed at Mt. Fuji. Simulation result is from the model HDSQI.

On the other hand, Fig. 12(b) may evoke much interest in the primary mass composition. As we learned from Table III, the effects due to primary mass composition are expected to be well reflected on the lateral spreads of gamma families with $N_c \geq 8$. Our experimental data is in substantial accord with the model HDSQI, which gives strong prima facie evidence to the assumption of heavy-enriched primary composition.

D. Correlation between multiplicity $\langle n' \rangle$ and lateral spread $\langle R \rangle$ of gamma rays

This correlation has been frequently discussed in connection with the violation of scaling in the fragmentation region. The results obtained at Mts. Kanbala and Fuji are presented in Fig. 14 together with the Pamir data,[18] comparing with the Monte Carlo results. It is worthwhile to note here that the mean lateral spreads of gamma rays in the families at Mt. Kanbala are on average larger by about 20% than those at Mt. Fuji because of low density of air. The same plots for the gamma families with $N_c \leq 5$ are shown in Fig. 15. In both figures, the experimental data at Mt. Kanbala and Mt. Fuji are consistent with the prediction of the model HDSQI. But the high multiplicity model may have no chance of reviving.

On the basis of a discrepancy between the Pamir data and their simulation result, the Pamir group asserts that scale breaking in the fragmentation region must be stronger than that seen in Fig. 2 and the shrinkage factor of x distribution R_s must be 3.0–5.0 (Ref. 18), still irreconcilable with our opinion. However, we feel that a few more words are called for on this subject since it is rather dangerous to discuss the validity of models based only on such a correlation. This is grounded on the fact that the value of n' is seriously affected by an error of energy determination of showers and also a spatial resolution of x-ray films especially for high-energy showers close to each other. In our experiments, together with high-sensitivity x-ray films, fine-grain x-ray films capable of measuring, with a reasonable accuracy, the position

and energy of showers in the central part of high-energy gamma families are used. The spatial resolution and error of energy determination for high-energy showers is estimated to be about 100 μm and 20%, respectively, at least in the energy region of $\sum E_\gamma$ less than several hundred TeV (Refs. 5 and 6). Such methodical problems must be examined critically.

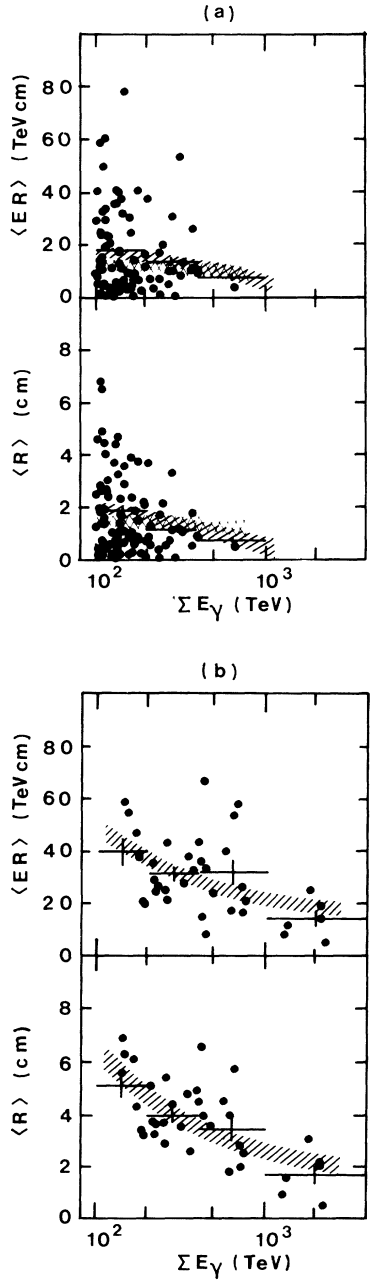

FIG. 12. (a) Scatter plots of lateral spreads of gamma rays, $\langle R \rangle$ and $\langle ER \rangle$, in the families consisting of $N_c \leq 5$ and gamma-family energy $\sum E_\gamma$, observed at Mt. Fuji. Simulation results from the models, HDSQI and PFQI and the experimental results are compared for their average values in respective region as those in Fig. 10. (b) Same as in (a), but in the case of gamma families consisting of $N_c \geq 8$.

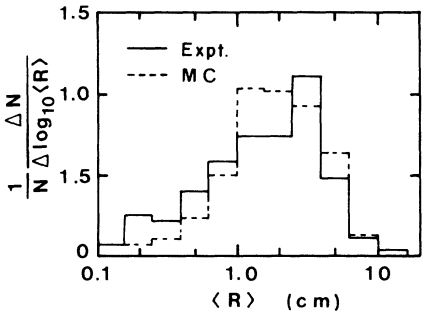

FIG. 13. Distribution of mean lateral spread $\langle R \rangle$ of each gamma family consisting of $N_c \leq 5$ in the energy region of $\sum E_\gamma = 100$–1000 TeV, observed at Mt. Fuji. The experimental data are compared with the simulation result from the model HDSQI.

E. Multicore structure of gamma families

In general gamma families are composed of several clusters. The size and number of clusters depends on the cutoff value χ_c introduced in Sec. IV. By increasing the value of χ_c one can cluster more and more particles. The clustering method was originally introduced to make it possible to pick out purely hadronic jet structure or high-P_t properties or effects due to the atomic mass of the primary. Here we discuss the cluster structure of gamma families to examine the effects of hadronic interactions and mass composition of primary cosmic rays. First the clustering is done to every gamma family according to the method described in Sec. III. After clustering, clusters with energies less than 10 TeV are excluded from the member of clusters in a family. To pick out gamma families with clear cluster or multicore structure preferentially, further conditions are imposed on the families after the above procedure: (1) $\sum E_\gamma \geq 100$ TeV; (2) $\sum E_c \geq 0.8 \sum E_\gamma$; (3) $\mathrm{Min}\{R_{ij},\ i<j,\ i$ and $j=1, 2, \ldots, N_c\} \geq a\mathrm{Max}\{\langle r_c \rangle^k,\ k=1,2,\ldots,N_c\}$, where $a=5$ and R_{ij} is the relative distance between the ith and jth cluster and $\langle r_c \rangle^k$ is the mean lateral spread of the kth

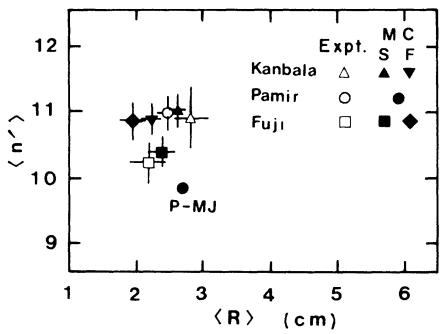

FIG. 14. Correlation of mean multiplicity $\langle n' \rangle$ and mean lateral spread $\langle R \rangle$ of gamma families, averaged in the energy region of $\sum E_\gamma = 200$–400 TeV. Pamir data are also plotted to compare with our results. The simulation results of the model HDSQI (labeled by S) and PFQI (F) are plotted for the comparison. For the scaling model P-MJ, see Ref. 18.

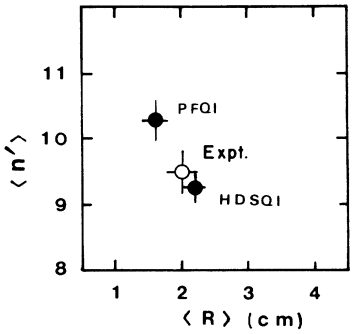

FIG. 15. Correlation of mean multiplicity $\langle n' \rangle$ and mean lateral spread $\langle R \rangle$ of gamma families consisting of $N_c \leq 5$, averaged over in the energy region of $\sum E_\gamma = 100$–1000 TeV. The experimental data from the Mt. Fuji experiment are compared with the simulation results from the models HDSQI and PFQI.

cluster. This is a smooth extension of the method adopted for selecting double-core events in previous papers.[2] For double cores ($N_c = 2$), the χ_{12} value is specially defined as $\chi_{12} = (E_1 E_2)^{1/2} R_{12}$. In this process the parameter value of $a = 5$ seems to become too rigorous when sorting is made on the superfamilies with $\sum E_\gamma \gtrsim 500$ TeV. Taking into account that the mean lateral spreads of gamma rays in the families decrease with increasing $\sum E_\gamma$ as seen in Figs. 10 and 12, the resolving parameter a should not be a constant, but a slowly decreasing function with $\sum E_\gamma$, for example, as $a = 5(\sum E_\gamma / 100\ \text{TeV})^{-\alpha}$ and $\alpha = 0.1$–0.15. But this problem will be taken up elsewhere otherwise our present discussion would go into particulars, disgressing slightly from the main subject.

In Fig. 16 is shown the number distribution of cores (clusters) relative to the total number of gamma families with $\sum E_\gamma \geq 100$ TeV. The energy flow spectrum of such multicore families is compared with the simulation results in Fig. 17. Here a deviation of the high-multiplicity model from the experiments becomes much clearer while the model HDSQI well reproduces the experimental results. The frequency of such multicore events in the energy region of $\sum E_\gamma \geq 100$ TeV is about 12% at both Mt. Kanbala and Mt. Fuji. On the other hand, the prediction by simulations is about 11% from the model HDSQI, but only 5% from the model PFQI. This means that the high-multiplicity model finds it hard to produce well-resolved multicore events at mountain altitudes.

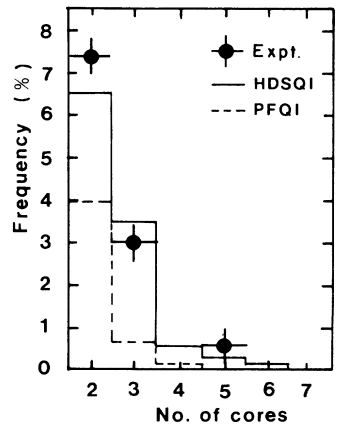

FIG. 16. Number of multicores in the gamma families with $\sum E_\gamma \geq 100$ TeV, selected by the criteria described in the text. The experimental data are compared with the simulation results of the HDSQI and PFQI models.

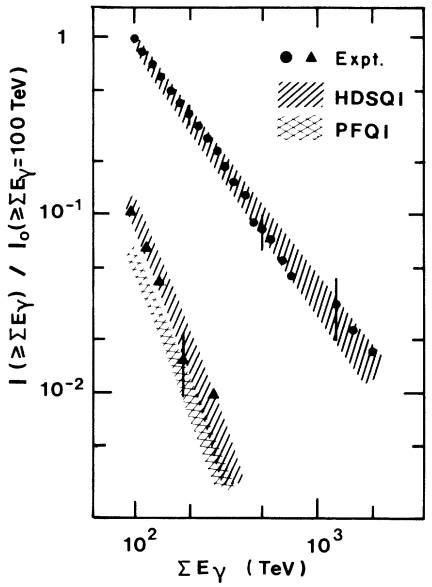

FIG. 17. Energy-flow spectrum of multicore families relative to that of all gamma families. Data are from the Mt. Fuji experiment. Simulation results from the HDSQI and PFQI models are also shown for comparison.

The effects of mass composition to such events are easily conjectured from the Monte Carlo simulation. We dissect the simulation results from the model HDSQI. To begin with, the fraction of primary species responsible for making gamma families with energy higher than 100 TeV at Mt. Kanbala is as follows, i.e., 72% by protons, 13% by helium nuclei, 15% by nuclei heavier than CNO and among this only 5% are by irons, despite assuming a heavy enriched primary (see Table I for a comparison). Referring to the multicore events, the fraction of protons increases up to 88%, but that of helium and nuclei heavier than CNO is only 8% and 4%, respectively. When focused only on double-core events, 94% are induced by proton components. On the other hand, the contribution of QCD jets to multicore events is estimated to be less than several percent in this energy region. Therefore, the multicore structures of gamma families appear to be valid for testing different models of hadronic interactions.

χ_{12} distribution of double-core events is presented in Fig. 18. The general tendency of experimental data obtained at Mts. Fuji and Kanbala is consistent with the model HDSQI. Here, the high-multiplicity model would be completely ruled out because of a difficulty of generating double-core events with large χ_{12} values, as discussed in previous papers.[2]

In a recent exposure at Mt. Kanbala we observed a peculiar double-core event named K5-618 with energy

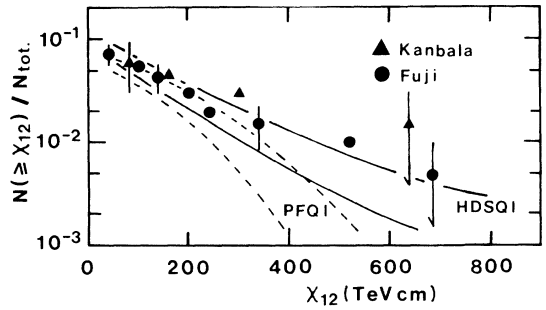

FIG. 18. χ_{12} distribution of double-core families with $\sum E_\gamma \geq 100$ TeV. Simulation results of the model HDSQI (area bounded by solid lines) and PFQI (area bounded by dotted lines) are presented to compare with the experimental data both by the Mt. Fuji and Mt. Kanbala experiments.

$\sum E_\gamma = 523$ TeV, zenith angle $= 27°$ and each core energy is $E_1 = 421$ TeV and $E_2 = 102$ TeV with a separation $R_{12} = 25.5$ cm. A chance probability of misidentifying two independent families as a double core is roughly estimated to be less than 2×10^{-3} if the inaccuracy of zenith angle measurement is smaller than 0.1 rad. Such energy-balanced double-core events may be picked up by imposing further conditions on the double-core criteria. The added requirement is that the energy of the main core (E_1) is higher than 100 TeV, the ratio of main (E_1) and subcore ($E_2 \leq E_1$), E_1/E_2, is less than 5 and $\chi_{12} \geq 100$ TeV cm. According to the Monte Carlo data, content of such kind of events in all double-core events is estimated to be about 14% at Mt. Fuji and 20% at Mt. Kanbala. The scatter plot of the energy sum $(E_1 + E_2)$ and the distance R_{12} of two cores is shown in Fig. 19. In this figure, some events observed at Mt. Pamir[18] and Mt. Chacaltaya[19] are also included. It is seen that almost all data are within the scope of Monte Carlo prediction. However, there are several events, including the event K5-618, falling in the region of $R_{12} > 20$ cm, far beyond the fluctuations of Monte Carlo simulation. According to the simulation calculation, by the way, a frequency of such events per double-core event depends on the relative distance as $0.3 R_{12}^{-\beta}$, where β takes the value ~ 1.3 at Mt. Kanbala and ~ 2.0 at Mt. Fuji and the expression is valid at $R_{12} \gtrsim 2$ cm. The existence of such events stimulates our interest considerably, but more data may be still needed to confirm that these events surely suggest new signs of hadronic interactions at ultrahigh-energy regions beyond fluctuations or chance probabilities.

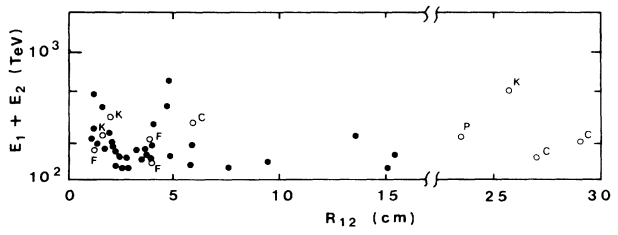

FIG. 19. Correlation between the sum energy $(E_1 + E_2)$ and the relative distance R_{12} of two cores. Simulation data (solid circles) of the model HDSQI are plotted in the figure, together with some data (open circles) from the Mt. Kanbala (K), Mt. Fuji (F), Mt. Chacaltaya (C), and Mt. Pamir (P) experiments.

VI. CONCLUSIONS

We have described gross features of gamma families observed with large-scale emulsion chambers which have been exposed both at Mt. Kanbala and at Mt. Fuji in comparison with the Monte Carlo simulations. It should be stressed here that the statistics of gamma-family data obtained at Mt. Fuji has been almost doubled since 1982 (Ref. 2), and moreover new data have been accumulated from the Kanbala experiment. These data obtained at different altitudes have been critically examined and compared to each other in order to get information about hadronic interactions as well as primary-cosmic-ray composition at energies around 10^{15}–10^{16} eV.

Both experiments show that the gross features of gamma families are wholly consistent with the assumption of approximate Feynman scaling in the fragmentation region. Of course we cannot say anything about behavior of particle production in the central region as this region is quite insensitive to the cosmic-ray propagation in the atmosphere. Some authors[16] are still claiming that the scaling in the fragmentation region is already strongly broken in the energy region around 10^{14} eV based on the pseudorapidity distributions obtained by CERN SPS Collider experiments.[3] However, accelerator data are limited only in the central region so that the speculation must be completely uncertain to the particle production in the fragmentation region. Actually their proposed model is shown to be none other than the fireball model examined in our simulation. In this paper we repeatedly showed that high-multiplicity model such as fireball is incompatible with gamma-family data especially in their lateral structures.

With the validity of approximate Feynman scaling in the fragmentation region, we can obtain the primary proton spectrum in the energy region around the "knee." The reason why we can get this is due to the fact, as discussed above, that the intensity of gamma families is very sensitive to the protons in the primary cosmic rays, i.e., more than 70% of families are generated by the collisions of protons even under the assumption of heavy-enriched primaries. This means that the ambiguity due to the contribution from nuclei with $Z \geq 2$ can be kept below 30% at the maximum estimate. With the aid of detailed Monte Carlo simulations as done in this paper, we can calculate a response function of gamma-family production. By using this response function, the primary proton spectrum is principally obtained, which is shown in Fig. 20. Studies by some authors[16,17] have reasoned a proton-dominant composition at the "knee" from analysis of air-shower data on muon and electrons and their fluctuations. Besides, a flattening rather than a steepening of the proton spectrum is invoked to account for all particle spectrum at energies around 10^{15}–10^{16} eV. As a matter of course, these contrast sharply with the implication from our experiments. Anyhow what should be stressed here is that such primary compositions never explain the flux of gamma families at mountain altitudes even if a

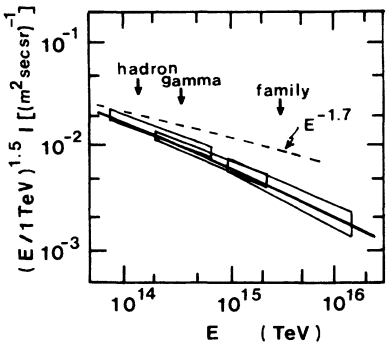

FIG. 20. Primary proton spectrum inferred from the gamma-family data observed at Mt. Kanbala and Mt. Fuji. The expected spectra (areas bounded by solid lines) from uncorrelated gamma-ray and hadron spectra (Ref. 5) are also shown in the same figure. The solid line shows the proton spectrum assumed in the heavy-enriched primary.

strong scaling violation is assumed in the fragmentation region. Some other air-shower experiments[20] support our conclusions. Details on the composition of primary cosmic rays will be discussed elsewhere.[21]

Our results and discussions are summarized as follows.

(1) Feynman scaling in the fragmentation region ($x \gtrsim 0.05$) is approximately valid at least up to the energies around 10^{16} eV. A part of mild scaling breaking seen there may be attributable to the frequent production of QCD jets.

(2) Inelastic cross sections continue to increase with energy as $\sigma_{in}(p\text{-air}) = 290(E_0/1\ \text{TeV})^{\delta}$ mb, where δ is estimated to be 0.06, at least up to energies around 10^{16} eV.

(3) The mean transverse momentum of secondaries is estimated to take a value of 500–550 MeV/c at energies around 10^{16} eV. QCD jet effect to the lateral spreads of gamma families is estimated to be no more than 10%. There exists no indication of rapidly increasing transverse momentum in the fragmentation region, say smaller than the above value.

(4) Multicore structures of gamma families are sensitive enough to rule out the high-multiplicity model.[17] QCD jets give a minor contribution to such structures of gamma families, say less than 10% in spite of a dramatic increasing of its cross sections.

(5) Our emulsion-chamber data seemingly favor the gradual decrease of protons in the primary at energies around the "knee." We suggest that the proton spectrum would start to bend at energies around 10^{14} eV. In other words, neither a flattening of the spectrum around 10^{14} eV, nor a hump around 10^{15} eV (Refs. 16 and 17) is inferred from our experiments. If the Grigorov all-particle data or air-shower data are trustworthy at energies around 10^{15} eV, then the fraction of protons and iron nuclei to the total is estimated to be 15–20 % and 30–40 %, respectively, at this energy region.[22]

The overall conclusions may be about the same as those in previous papers.[2] Here an emphasis should be, however, placed upon the fact that these conclusions have been much strengthened in comparing both the sufficient data at Mt. Fuji and the new data at Mt. Kanbala of different altitudes with the Monte Carlo simulations which are refined to the latest ones as shown in Sec. III.

In this paper we presented only the general features of gamma families with energies of $\sum E_\gamma = 100$–3000 TeV, and showed which pictures about hadronic interactions and primary composition are totally compatible with our data. However, one should note here that there actually exist some instances of events beyond the fluctuations expected from our Monte Carlo simulation. These will be critically checked elsewhere. But it is also important to note that these phenomena never change the general properties of hadronic interactions mentioned above.

Characteristic features of hadron families[7] and superfamilies accompanying "halo"[23] will be discussed in separate papers.

ACKNOWLEDGMENTS

The work at Mt. Kanbala was supported by grants from Academia Sinica in China and Japanese Ministry of Education including the Grant in Aid for Overseas Scientific Survey. Also, the Japanese authors would like to express their thanks to Sengen Shrine and the Kawaguchiko Office of the Agency of Environmental Maintenance for extending to them every facility necessary for carrying out the experiment at Mt. Fuji. Data analysis and Monte Carlo calculation were made with the computer FACOM M380 of the Institute of Nuclear Study, University of Tokyo.

[1]J. R. Ren *et al.*, in *Proceedings of the International Symposium on Cosmic Rays and Particle Physics,* Tokyo, Japan, 1984, edited by A. Ohsawa and T. Yuda (Institute for Cosmic Ray Research, University of Tokyo, Tokyo, 1984), p. 87; in *Proceedings of the Nineteenth International Cosmic Ray Conference,* La Jolla, California, 1985, edited by F. C. Jones, J. Adams, and G. M. Mason (NASA Conf. Publ. No. 2376) (Goddard Space Flight Center, Greenbelt, MD, 1985), Vol. 6, p. 439.

[2]M. Akashi *et al.*, Phys. Rev. D **24**, 2353 (1981); M. Amenomori *et al.*, *ibid.* **25**, 2807 (1982); in *Proceedings of the Twentieth International Cosmic Ray Conference,* Moscow, 1987, edited by V. L. Kozyarivsky *et al.* (Nauka, Moscow, 1987), Vol. 5, p. 379.

[3]UA5 Collaboration, K. Alpgard *et al.*, Phys. Lett. **121B**, 209 (1983); UA1 Collaboration, A. Arnison *et al.*, *ibid.* **123B**, 167 (1983); J. G. Rushbrooke, Report No. CERN-EP/85-178, 1985 (unpublished); UA5 Collaboration, G. J. Alner *et al.*, Z. Phys. C **33**, 1 (1986).

[4]J. R. Ren *et al.*, in *Proceedings of the Twentieth International Cosmic Ray Conference* (Ref. 2), Vol. 5, p. 321; J. A. Chinellato *et al.*, *ibid.*, p. 359; S. Yamashita, J. Phys. Soc. Jpn. **54**, 529 (1985); A. S. Borisov *et al.*, in *Proceedings of the International Symposium on Cosmic Rays and Particle Physics* (Ref. 1), p.

3; M. Amenomori *et al.*, *ibid.*, p. 76; M. Akashi *et al.*, Nuovo Cimento **67A**, 221 (1982).

[5]M. Amenomori *et al.*, in *Proceedings of the Nineteenth International Cosmic Ray Conference* (Ref. 1), Vol. 2, p. 206; J. R. Ren *et al.*, Nuovo Cimento **10C**, 43 (1987).

[6]M. Akashi *et al.*, Nuovo Cimento **65A**, 355 (1982); M. Amenomori *et al.*, in *Eighteenth International Cosmic Ray Conference, Bangalore, India, 1983, Conference Papers*, edited by N. Durgaprasad *et al.* (Tata Institute of Fundamental Physics, Bombay, 1983), Vol. 11, p. 57.

[7]J. R. Ren *et al.*, following paper, Phys. Rev. D **38**, 1417 (1988).

[8]L. K. Ding, N. Hotta, K. Kasahara, T. Yuda, and S. Torii, in *Proceedings of the International Symposium on Cosmic Rays and Particle Physics* (Ref. 1), p. 142; L. K. Ding, K. Kasahara, S. Torii, and T. Yuda, Institute for Cosmic Ray Research, University of Tokyo, Report No. 107-87-1, 1983 (unpublished).

[9]T. Kafka *et al.*, Phys. Rev. D **16**, 1261 (1977).

[10]M. Simon *et al.*, Astrophys. J. **239**, 712 (1980); T. H. Burnett *et al.*, Phys. Rev. Lett. **51**, 1010 (1983); in *Proceedings of the Nineteenth International Cosmic Ray Conference* (Ref. 1), Vol. 2, p. 48.

[11]M. Nagano *et al.*, J. Phys. G **10**, 1295 (1984).

[12]W. R. Webber, *Composition and Origin of Cosmic Rays* (Reidel, Dordrecht, 1983), p. 25.

[13]C. J. Cesarsky and P. O. Lagage, in *Proceedings of the Seventeenth International Cosmic Ray Conference,* Paris, France, 1981 (Centre d'Études Nuclaires, Saclay, 1981), Vol. 2, p. 335; W. I. Axford, *ibid.*, Vol. 12, p. 155.

[14]N. L. Grigorov *et al.*, in *Proceedings of the Twelfth International Cosmic Ray Conference,* Hobart, 1971, edited by A. G. Fenton and K. B. Fenton (University of Tasmania Press, Hobart, Tasmania, 1971), Vol. 5, p. 1746.

[15]M. Shibata, Phys. Rev. D **24**, 1847 (1981).

[16]J. Linsley, in *Eighteenth International Cosmic Ray Conference, Bangalore, India, 1983, Conference Papers* (Ref. 6), Vol. 12, p. 135; C. Fichtel and J. Linsley, Astrophys. J. **300**, 474 (1986).

[17]J. Wdowczyk and A. W. Wolfendale, Nature (London) **306**, 347 (1983); J. Phys. G **13**, 411 (1987).

[18]S. A. Slavatinsky, in *Proceedings of the International Symposium on Cosmic Rays and Particle Physics* (Ref. 1), p. 700; A. M. Dunaevsky, in *Proceedings of the International Symposium on Cosmic Ray Superhigh Energy Interactions,* Beijing, 1986, edited by L. K. Ding, H. H. Kuang, and J. R. Ren (Institute of High Energy Physics, Academia Sinica, 1986), pp. 1–103.

[19]J. Bellandi *et al.*, in *Cosmic Rays and Particle Physics—1978,* proceedings of the Bartol Conference, edited by T. K. Gaisser (AIP Conf. Proc. No. 49) (AIP, New York, 1979), p. 145.

[20]J. A. Goodman *et al.*, Phys. Rev. D **26**, 1043 (1982); V. K. Balasubrahmanyan, B. V. Sreekantan, J. A. Goodman, and G. B. Yodh, in *Proceedings of the International Symposium on Cosmic Ray Superhigh Energy Interactions* (Ref. 18), pp. 6–1; M. Nagano *et al.*, J. Phys. G **10**, 235L (1984).

[21]M. Amenomori *et al.*, in *Proceedings of the Twentieth International Cosmic Ray Conference* (Ref. 2), Vol. 1, p. 386.

[22]In 1981, the Mt. Fuji Collaboration estimated less protons and more heavy nuclei than this fraction at the same energy region as the articles in Ref. 2. At that time they used rather old interaction models without QCD jets in the Monte Carlo simulation. Also, in 1983 the energies of all showers observed were increased on average by about 30% based on the calibration excpreiment of emulsion chambers using accelerator beams (see Ref. 6). Then a difference with the fraction estimated in 1981 could be attributed to these reasons.

[23]J. R. Ren *et al.*, Phys. Rev. D **38**, 1426 (1988).

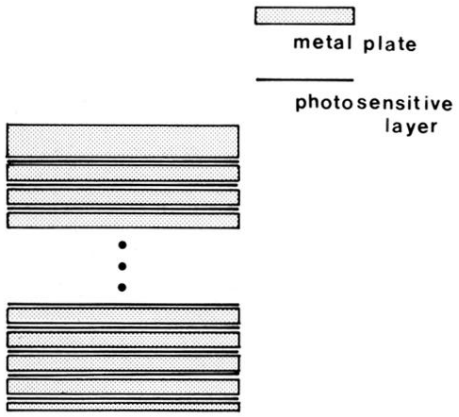

FIG. 1. The typical structure of an emulsion chamber.